Electronic Supplementary Material (ESI) for Nanoscale Advances.

<Electronic Supplementary Information>

Chemical and Topographical Patterns Combined with Solution Shear for Selected-Area Deposition of Highly-Aligned Semiconducting Carbon Nanotubes

Jonathan H. Dwyer,[a] Anjali Suresh,[b] Katherine R. Jinkins,[b] Xiaoqi Zheng,[b] Michael S. Arnold,*[b] Arganthaël Berson,*[c] and Padma Gopalan*[a,b]

a. Department of Chemical and Biological Engineering, University of Wisconsin-Madison, 1415 Engineering Drive, Madison, WI 53706, United States

b. Department of Materials Science and Engineering, University of Wisconsin-Madison, 1509 University Avenue, Madison, WI 53706, United States. E-mail: pgopalan@wisc.edu

c. Multiphase Flow Visualization and Analysis Laboratory (MFVAL), University of Wisconsin-Madison, 1500 Engineering Drive, Madison, WI 53706, United States. E-mail: arganthael.berson@wisc.edu

Table of Contents

Electron Beam Resist Stability during OTS Deposition

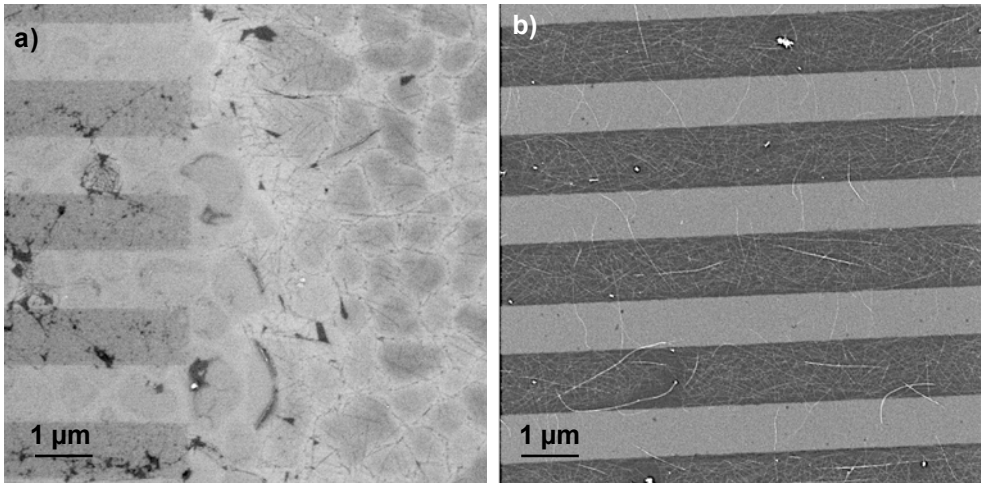

Figure S1. SEM images of CNTs deposited on OTS (bright) lines fabricated on SiO_2 (dark) using (a) PMMA and (b) ma-N 2401 electron beam resists. PMMA shows OTS penetration during deposition while the ma-N shows no OTS penetration. Scale bar is 1 µm for both images.

Characterization of Carbon Nanotube (CNT) Alignment using Two-Dimensional Fast Fourier Transform (2D FFT) Method

Most commonly, alignment degree of s-CNTs is quantified using polarized Raman spectroscopy.[1-3] Polarized Raman spectroscopy is capable of measuring the CNT G-band[4] around 1590 cm^{-1} at different orientations to analyze CNT anisotropy, which is then reported as the standard deviation (σ) by assuming a Gaussian distribution. However, polarized Raman measurements were not fully applicable to the s-CNT arrays fabricated in this study for a few reasons. First, Raman peak intensities are substrate dependent,[5] meaning that a s-CNT residing on a different chemical environment will give a different Raman intensity. These intensity discrepancies would result in an inaccurate characterization of the s-CNT alignment degree. Second, manual measurement from SEM images showed that the orientation distribution of our s-CNT arrays deviates slightly from a

normal distribution. For example, the small non-zero background, or tail, in the distribution that can be seen in Figure S2 will skew the calculation of σ from polarized Raman spectroscopy resulting in significantly incorrect s-CNT alignment degrees. Third, the smallest width patterns (100 nm wide) cause Raman laser interference from surface pattern grating effects,[6] leading to inaccurate values. Hence, the s-CNT alignment was characterized by performing a two-dimensional fast Fourier transform (2D FFT) analysis of SEM images for the deposited s-CNT arrays.

The alignment of the carbon nanotube arrays is characterized by performing a two-dimensional fast Fourier transform (2D FFT) analysis of scanning electron microscopy (SEM) images of the deposited arrays. The method has been used in the literature for characterizing the alignment of various types of fibrous materials[7, 8] including CNT arrays[9]. The analysis procedure is similar to that described by Brandley *et al.*[9] and adapted to account for the presence of topographical trenches. The following steps were followed for the 2D FFT analysis:

- First, an SEM image of the CNT array is prepared for analysis (see Figure S3a). The mesas between trenches are removed from the image, and the images of the trenches are ``stitched'' together into a single image (see Figure S3b). Removing the mesas reduces noise and reduces the amplitude of a large bright peak at low frequency in the FFT image that could overwhelm the desired signal from the CNT array.
- Second, the 2D FFT of the prepared image is calculated using the *fft2* function in Matlab^{tm} (see Figure S3c). The FFT is shifted to the center of the image using the *fftshift* function in Matlab^{tm} for a more convenient representation. The FFT shows a pattern of bright lobes oriented perpendicular to the main direction of orientation of the CNT array.

- Finally, the orientation distribution is obtained by integrating the intensity of the shifted FFT from a distance f_{min} to a distance f_{max} from the center of the image, at angles varying from -90° and 90° (see Figure S3d). In practice, the image is rotated using the function *imrotate* in Matlab[tm] at each angle of interest using a nearest-neighbor interpolation scheme. The intensity is averaged over the horizontal axis from f_{min} to f_{max}. Bright peaks at spatial frequencies below f_{min} = N/($2t_{min}$), where N represents the number of pixels and t_{min} is the minimum pixel threshold, correspond to large scale fluctuations associated, for example, with uneven illumination or stitching of multiple trench images. Spatial frequencies above f_{max} = N/($2t_{max}$), where t_{max} is the maximum pixel threshold, correspond to speckle noise. We verified that small changes to the values of f_{min} and f_{max} affect the measured σ of the fiber distribution by less than 1°. In general, we found that t_{min} = 10 pixels and t_{min} = 2 pixels worked well for most of our images. Finally, the orientation distribution is fitted with a Gaussian distribution to obtain σ (see Figure S3e).

The 2D FFT method is limited to orientation distributions that are fully contained within the range -90° to 90°. For a normal distribution, this means that results will not be accurate for arrays with a standard deviation greater than approximately 30°. At greater standard deviations, only a fraction of the orientation distribution is known. Because the baseline value (the offset value that would be returned by the 2D FFT algorithm for a zero probability at a given angle – this value is never zero in practice and is affected by noise in the images) is unknown, it is impossible to obtain a curve fitting of the orientation distribution with accuracy. In our measurements, only two data points (at a low shear rate of 46 s^{-1} for bulk and 2000 nm wide trenches, see SI Figure S7) have an orientation distribution with a standard deviation greater than 30°. Visual inspection of the SEM images for these two cases confirm that the CNT array shows virtually no preferential direction of alignment.

The 2D FFT method was validated by comparing its results with orientation distributions obtained by manual counting of individual nanotubes for a selection of images. In all the tested images, the 2D FFT method tends to overestimate the standard deviation of the orientation distribution with an error of no more than 5°.

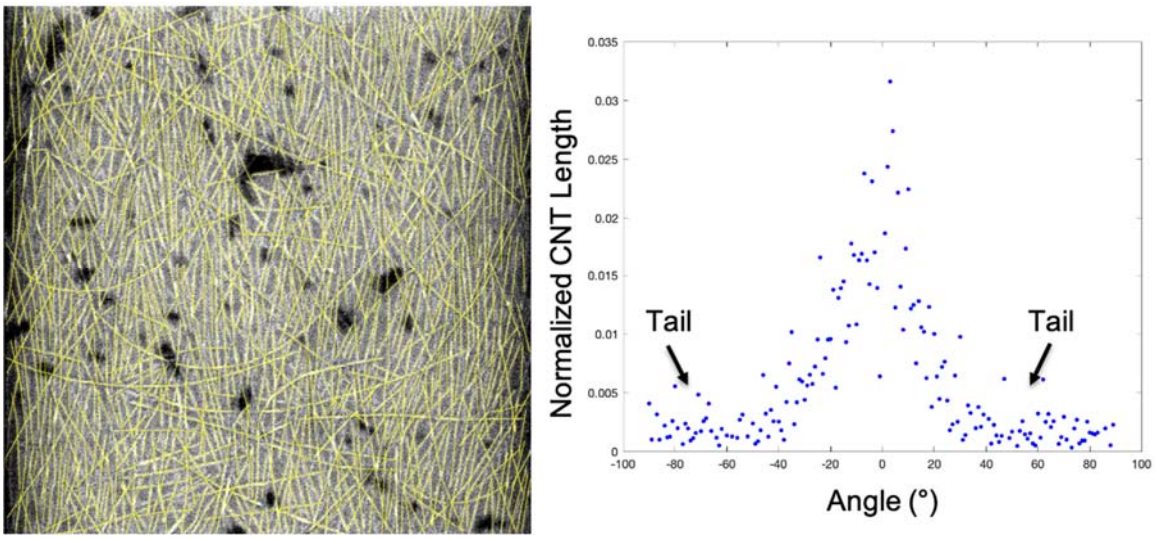

Figure S2. Manual calculation of CNT orientation from SEM image (left). Plot (right) illustrates CNT orientation distribution normalized to CNT length. Arrows point to tails in distribution that deviate from a normal distribution.

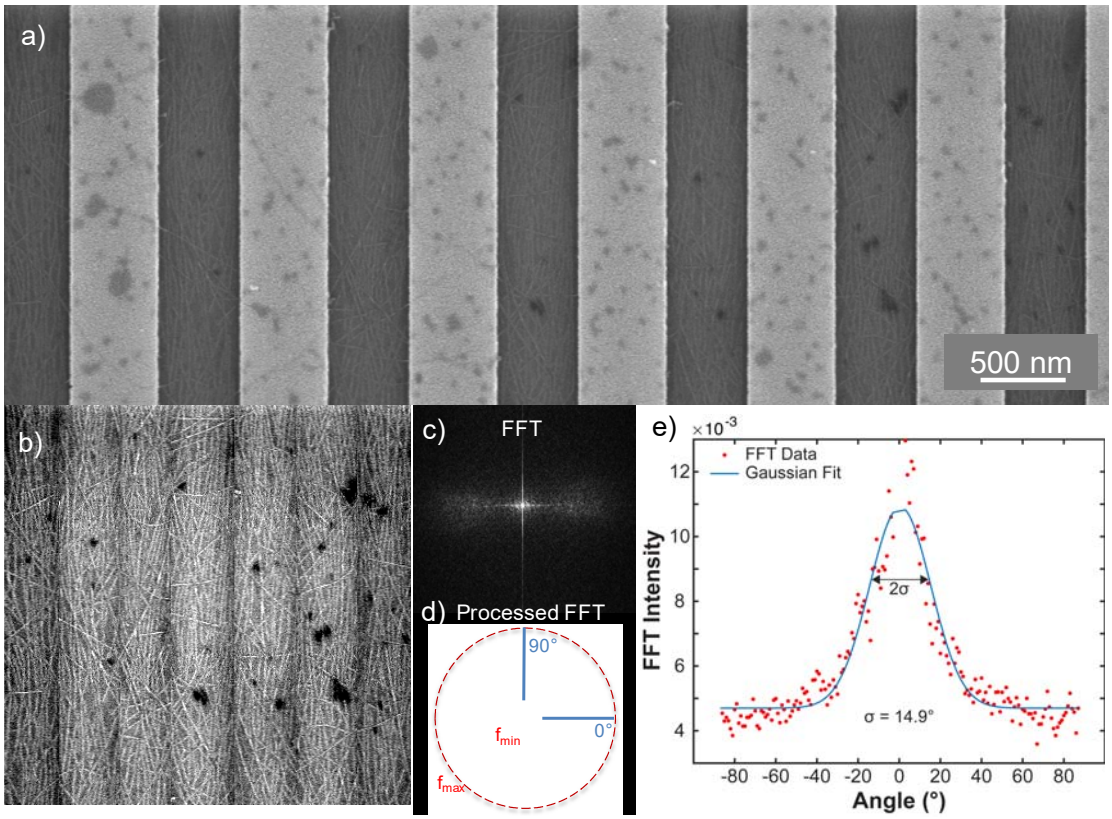

Figure S3. Two-dimensional fast Fourier transform (2D FFT) methodology used to quantify s-CNT alignment in arrays. (a) SEM image of 500 nm wide s-CNT arrays (dark stripes) spaced 500 nm apart from surface pattern (bright stripes). (b) SEM image of s-CNT arrays from image (a) stitched together. (c) 2D FFT of s-CNT arrays in image (b). (d) Processed 2D FFT defining the minimum (f_{min}) and maximum (f_{max}) frequencies in red due to small scale noise and large scale fluctuations due, for example, to uneven image illumination. Blue lines show angles corresponding to 0 and 90 degrees in FFT, where 0 degrees in the FFT corresponds to vertical alignment in the SEM image. (e) Orientation distribution from 2D FFT (red points) shown in (d) obtained by integrating the FFT intensity radially from f_{min} to f_{max}, for all angles between -90 to 90 degrees. Blue line is Gaussian curve fit of data, which outputs a standard deviation (σ) used as our s-CNT alignment degree.

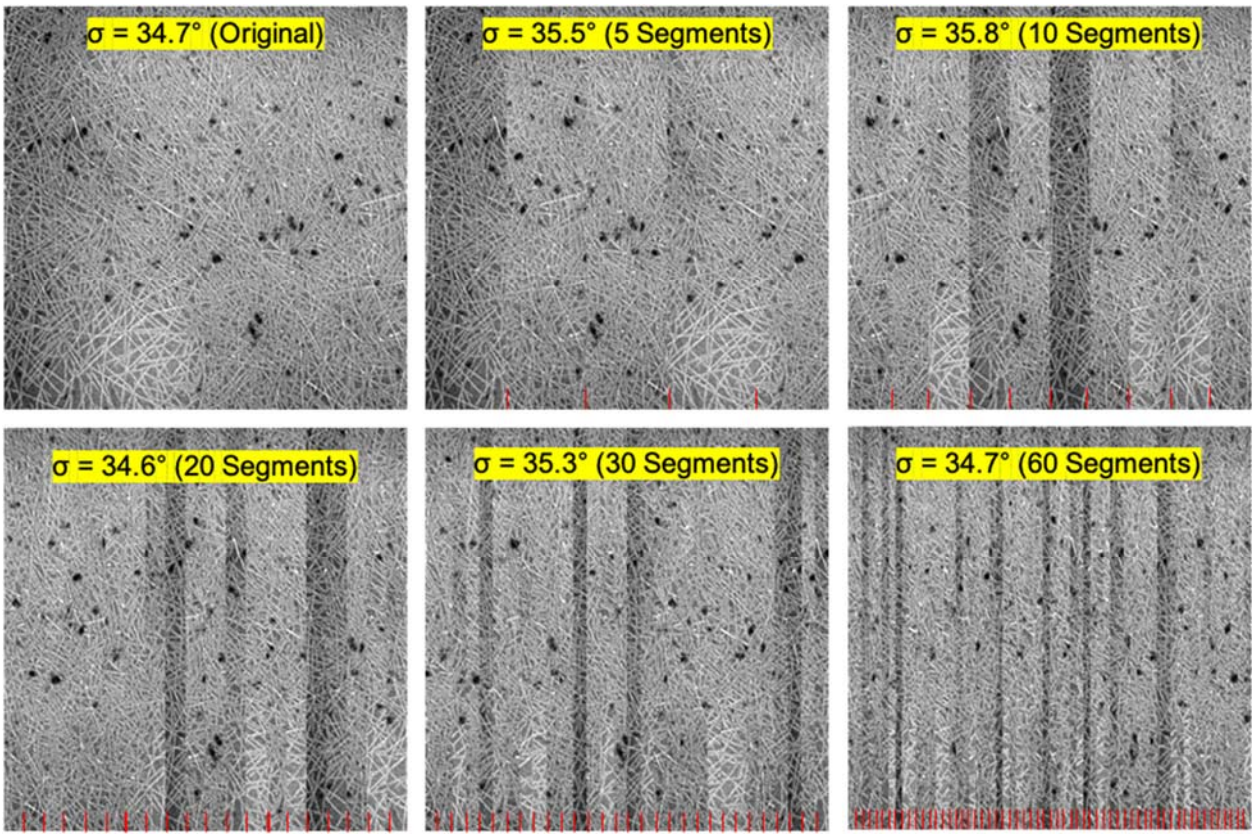

Figure S4. SEM images showing that the number of times images are stitched together does not impact the resulting standard deviation by more than ~ 1°. CNTs were deposited at a shear rate 46 s^{-1} using 375 µL s-CNT chloroform ink at a concentration of 240 µg/mL.

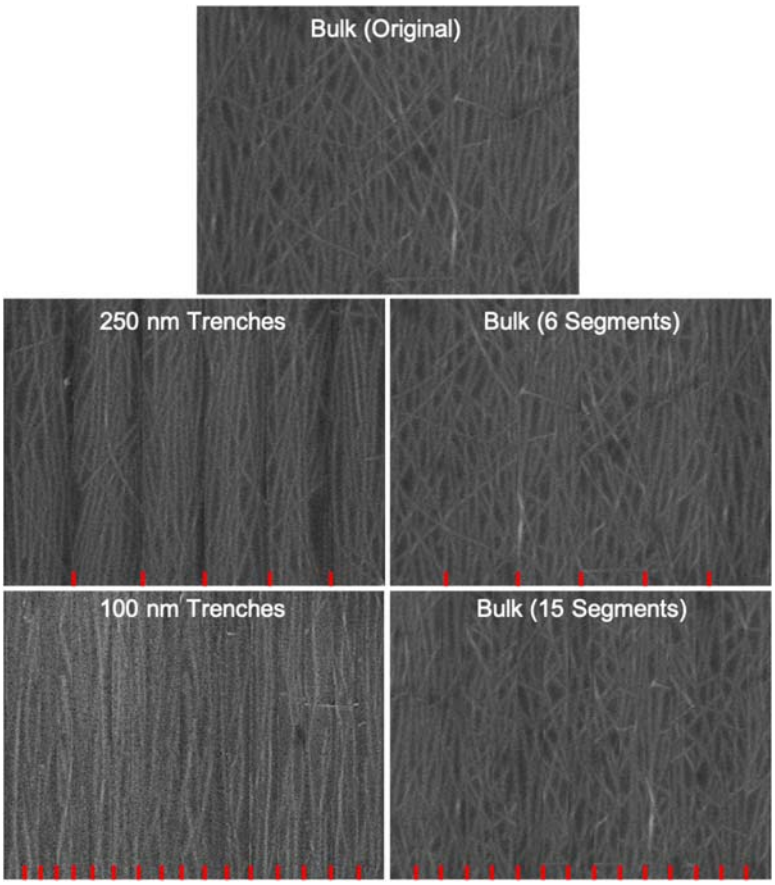

Figure S5. SEM images showing that stitching together the narrower trenches does not increase the appearance of improved CNT alignment. The bulk top image is the original image. It is split into 6 segments (middle right) like the 250 nm trenches (middle left) and into 15 segments (bottom right) like the 100 nm trenches (bottom left). CNTs were deposited at a shear rate 4,600 s^{-1} using 375 µL s-CNT chloroform ink at a concentration of 240 µg/mL.

Alignment degree of CNTs in Chemical Patterns

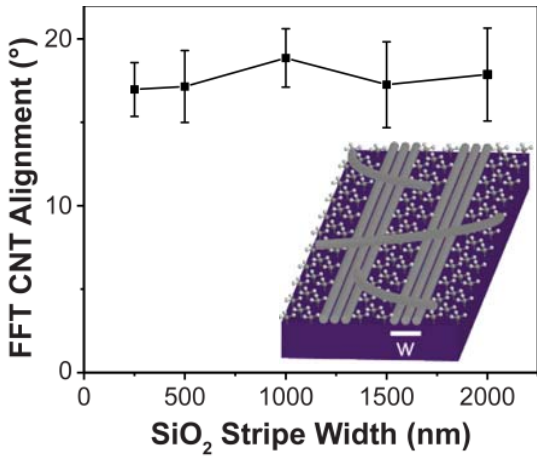

Figure S6. Plot of s-CNT alignment degree quantified using standard deviation (σ) from FFT analysis for different SiO_2 stripe widths *w* in the chemical pattern. Cartoon in bottom right of plot illustrates the chemically patterned substrate and the deposited CNTs on which FFT analysis was performed.

Effect of OTS Width on CNT Alignment

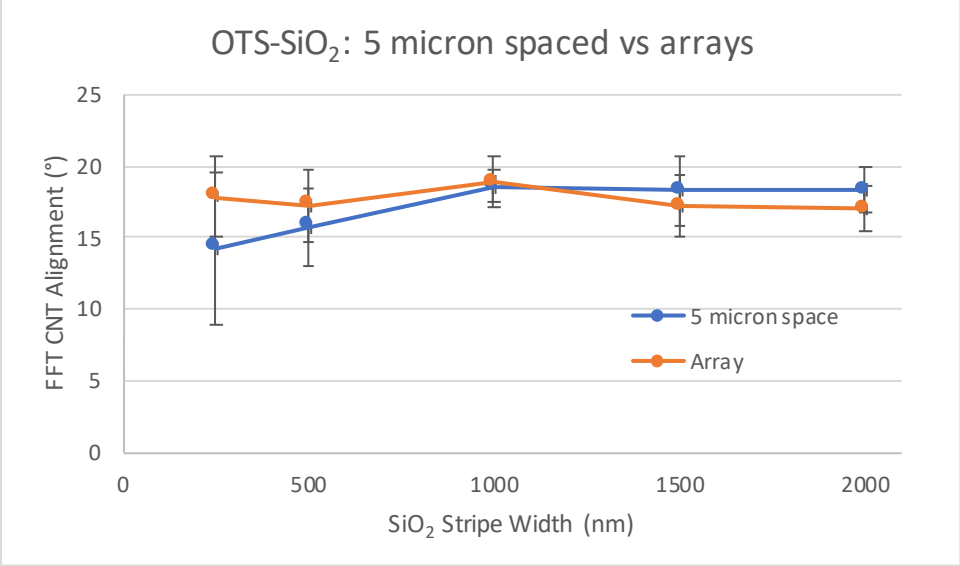

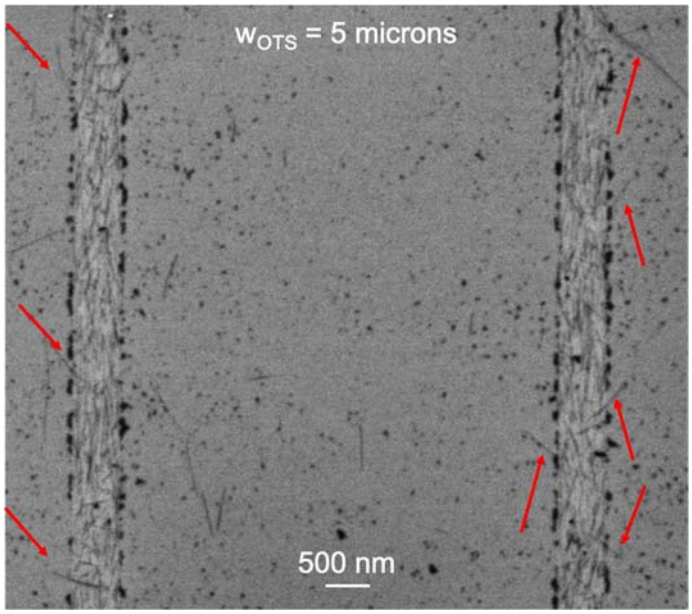

Figure S7. Plot of s-CNT alignment degree (standard deviation) as a function of the width of SiO_2 stripes where OTS stripe widths were either (blue) 5 microns or (orange) the same as SiO_2 stripe width *w*. SEM image below shows 500 nm wide SiO_2 stripes when OTS stripe width is 5 microns. Red arrows point to CNTs that are pinned to SiO_2 stripes and partially deposited on nearby OTS regions. See Figure 1a in main text for fabrication procedure.

CNT Deposition Behavior on Chemical + Topographical Patterns

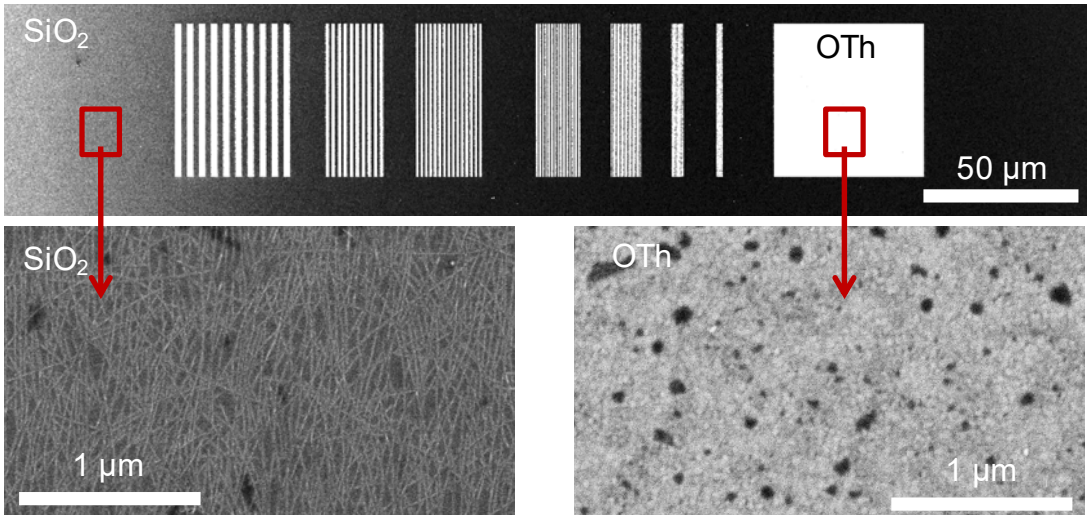

Figure S8. SEM images of CNTs deposited on OTh-grafted gold surface compared to on SiO_2. CNTs were deposited using 375 µL of 240 µg/mL solution in chloroform at a shear rate of 46,000 s^{-1}.

Sidewall Composition Effect on CNT Density

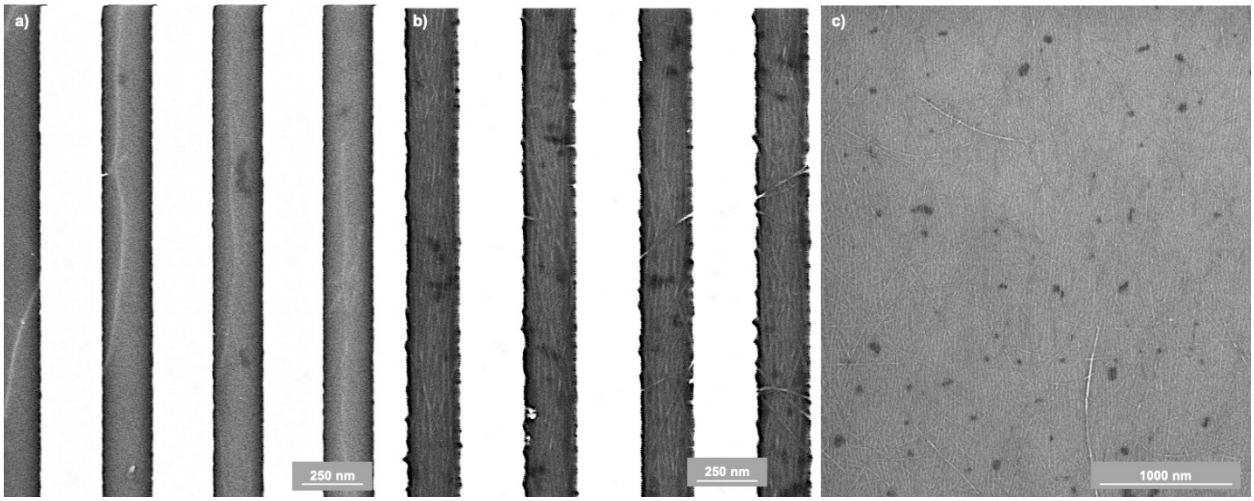

Figure S9. SEM images showing the CNT arrays on stripes in between 40 nm tall OTh functionalized Au/Cr stack when the stack composition is (a) 2.5 nm Cr and 37.5 nm Au on top, and (b) 37.5 nm Cr and 2.5 nm Au on top. (c) SEM image of CNT deposition on bulk SiO_2 away from patterns.

CNT Density in Chemical + Topographical Patterns

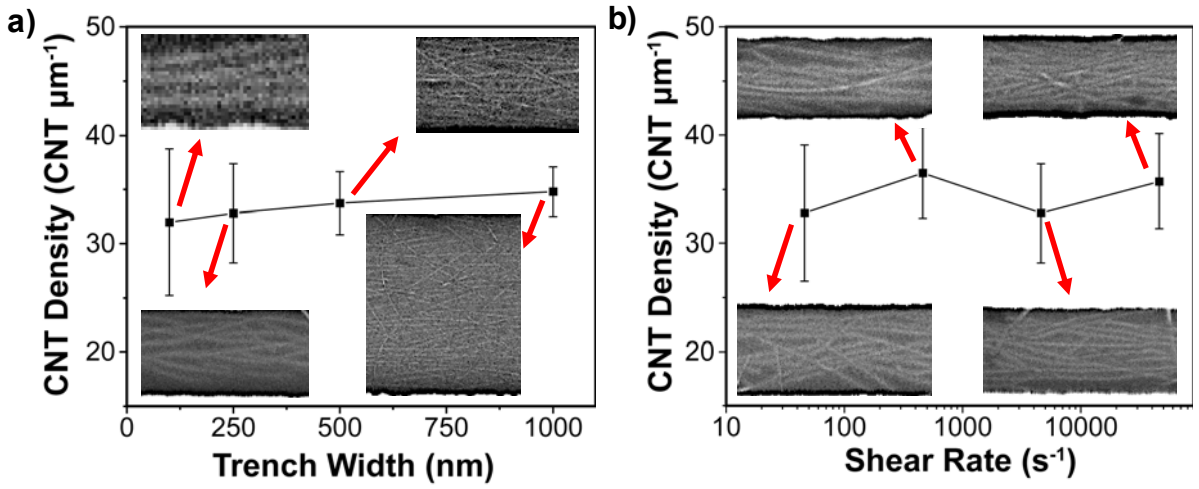

Figure S10. Plots of CNT density (CNTs μm^{-1}) versus: (a) trench width *w* at constant 4,600 s^{-1} shear rate, and (b) shear rate at constant *w* of 250 nm. Insets in both plots are representative SEM images of corresponding data points. CNT density was obtained by counting the CNTs along the CNT diameter axis to generate the reported linear density. Five measurements were made over three samples to generate each data point and error bars on the plots.

Low Shear Rate Random CNT Alignment

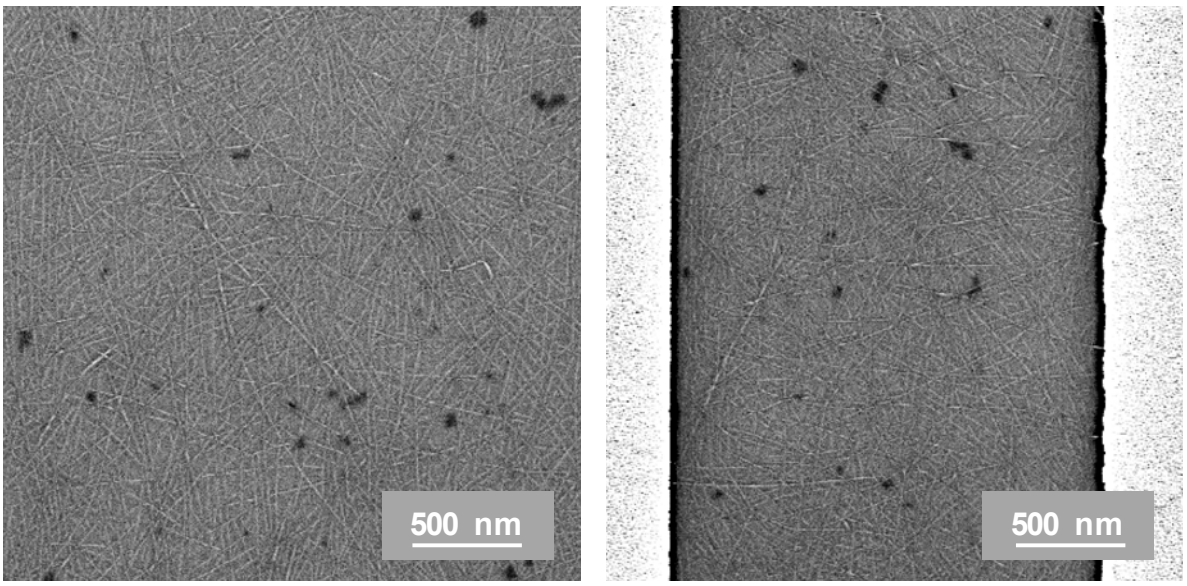

Figure S11. SEM images of s-CNT deposited at 46 s^{-1} shear rate on bulk (planar) SiO_2 (left) and 2000 nm wide OTh-grafted trenches (right). Both visually show a non-preferential orientation to deposition direction 2D FFT analysis could not accurately fit these images because the standard deviation was greater than the 30° limit.

Low Shear Rate Confinement Effect

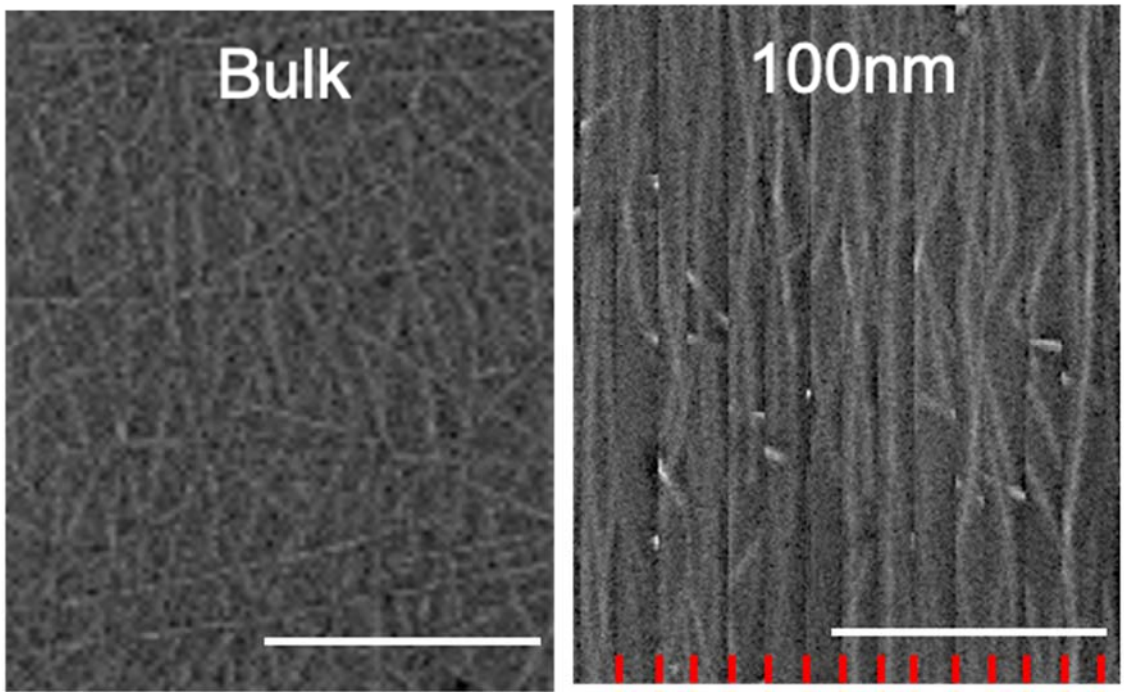

Figure S12. SEM images of s-CNT deposition at 46 s^{-1} shear rate using 375 µL s-CNT chloroform ink at a concentration of 240 µg/mL. Images are on (left) planar SiO_2 (bulk) and (right) in 100 nm trench. Right image is multiple 100 nm trenches stitched together used for 2D FFT analysis. Scale bar is 500 nm for both images.

Metal Trench Height Effects

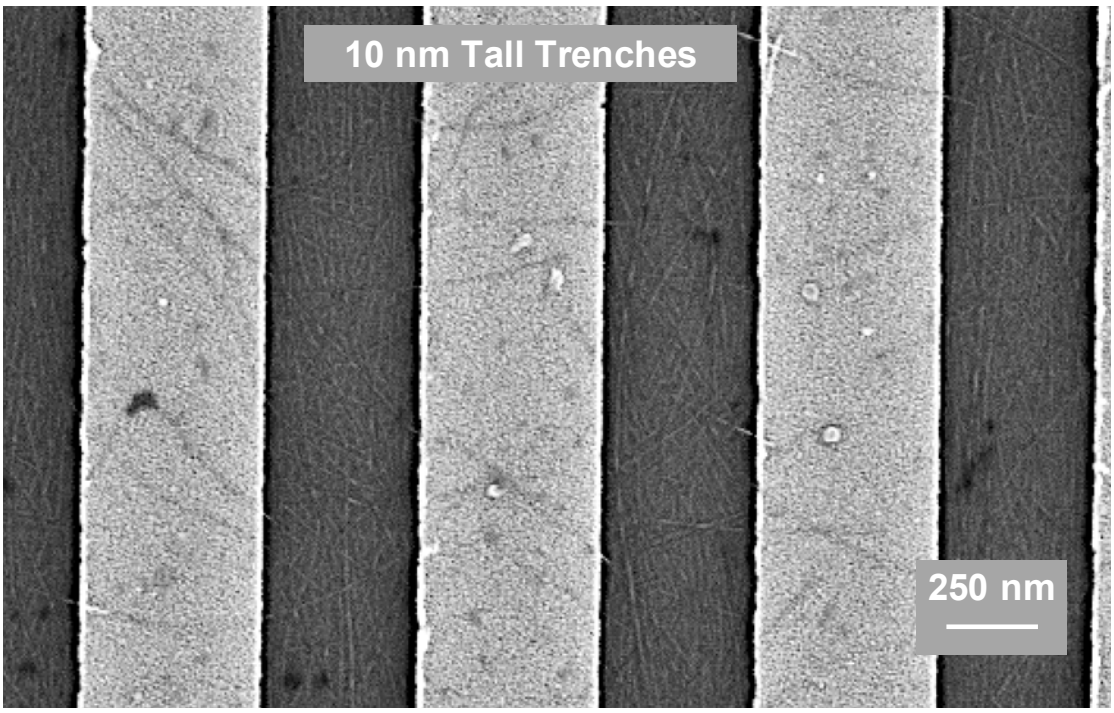

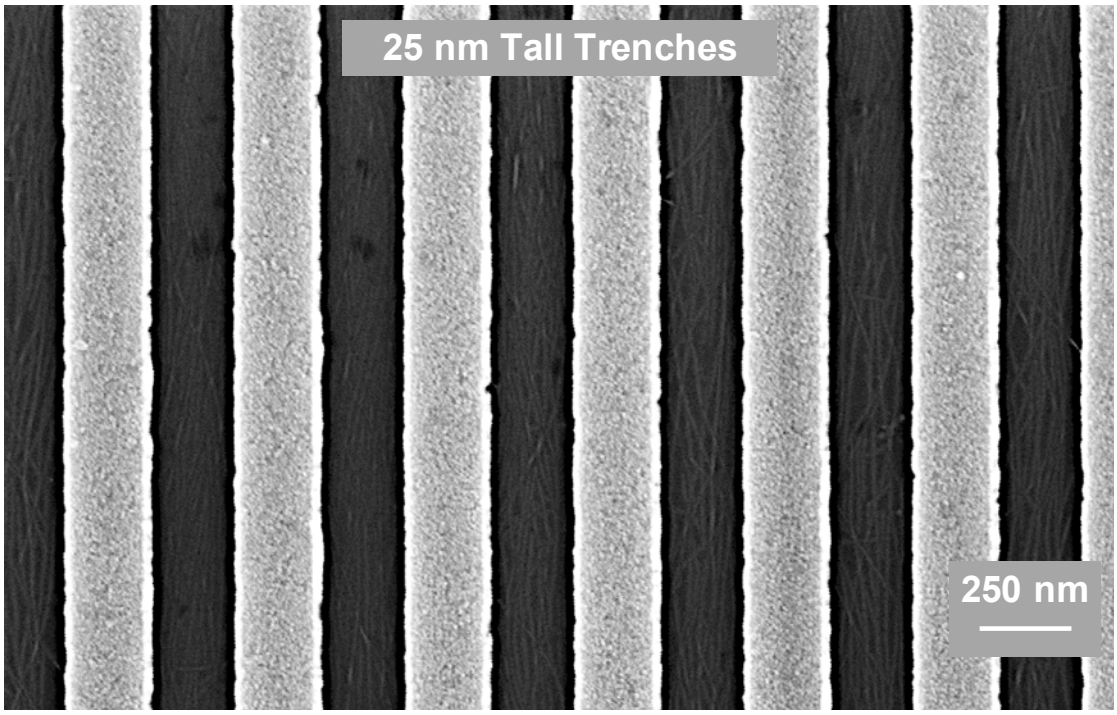

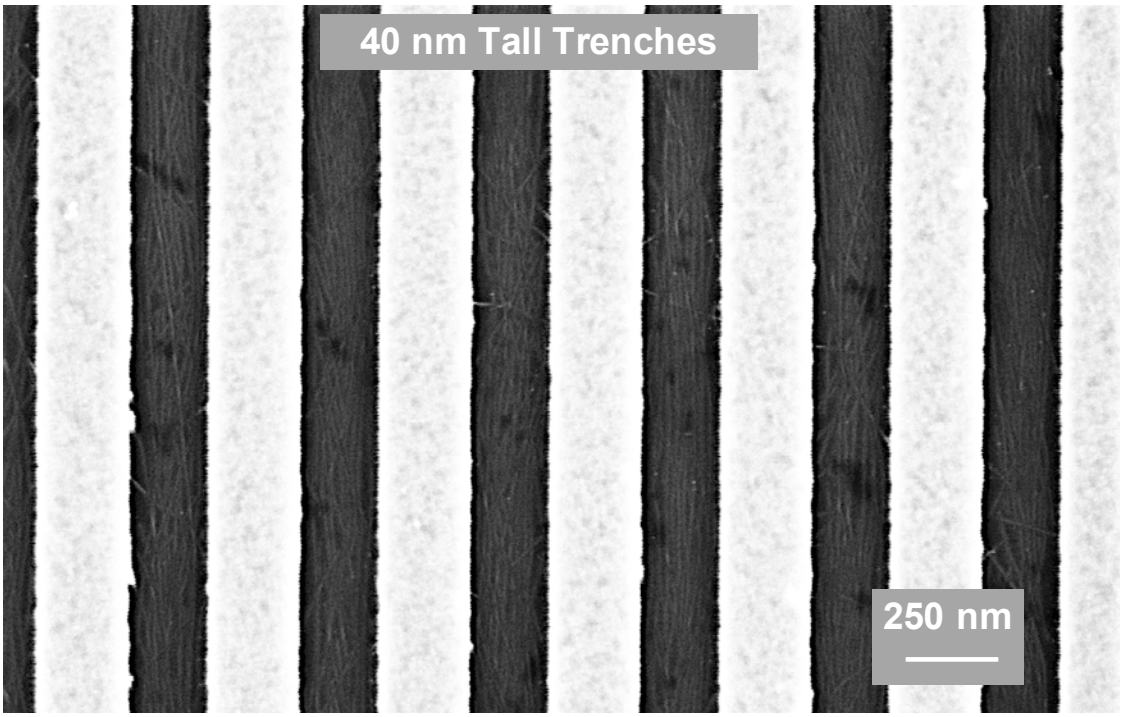

Figure S13. SEM images of s-CNT arrays deposited at a shear rate 4,600 s^{-1} using 375 µL s-CNT chloroform ink at a concentration of 240 µg/mL on chemical + topographical patterns where the trench width is 250 nm and trench walls are 10, 25, and 40 nm tall. Top SEM image shows increased CNT bridging across 10 nm stripes compared to 25 and 40 nm tall trenches. All trench compositions comprised of 2.5 nm Au on top and remainder Cr.

Large Area CNT Deposition

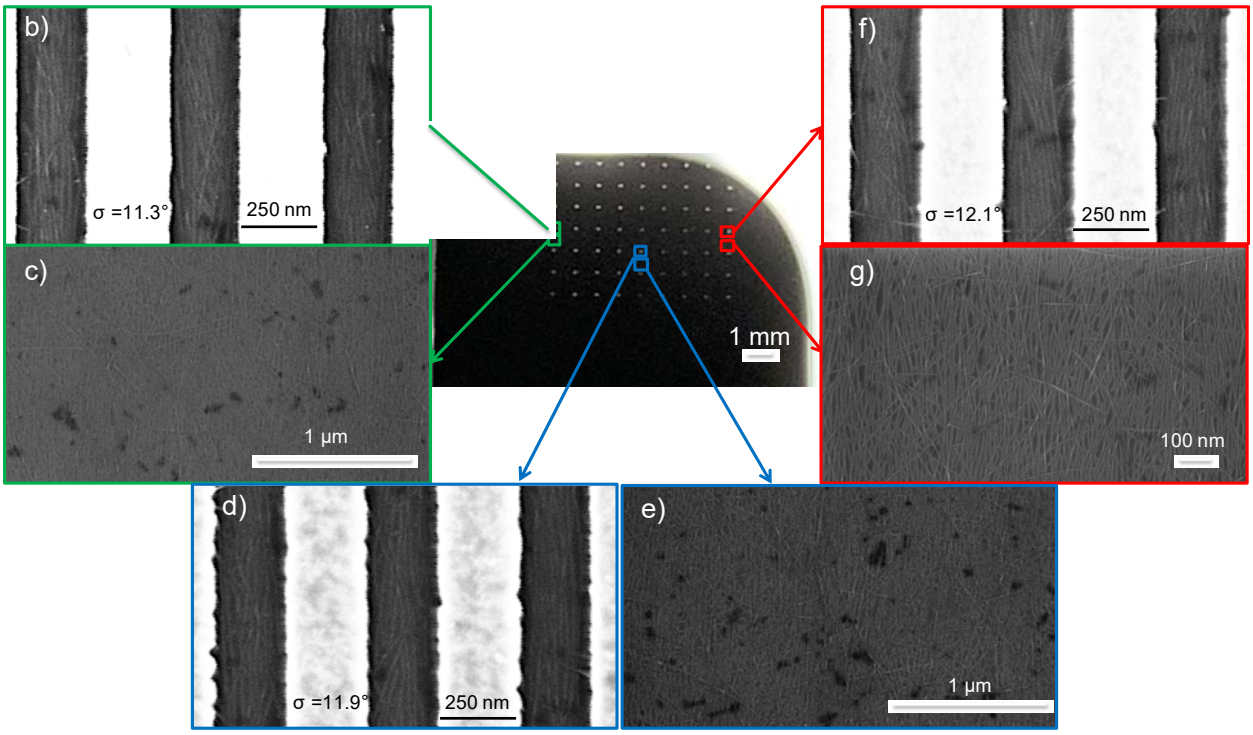

Figure S14. CNT deposition over 2 × 3 cm^2 SiO_2/Si substrate. (a) Optical image of patterned region. (b-g) SEM images of different regions of the substrate. (b,d,f) 250 nm wide trenches with the CNT alignment degree (σ) for each image reported in the bottom left. (c,e,g) Bulk CNT deposition near the patterned region.

Effect of Trench Removal on CNT Alignment

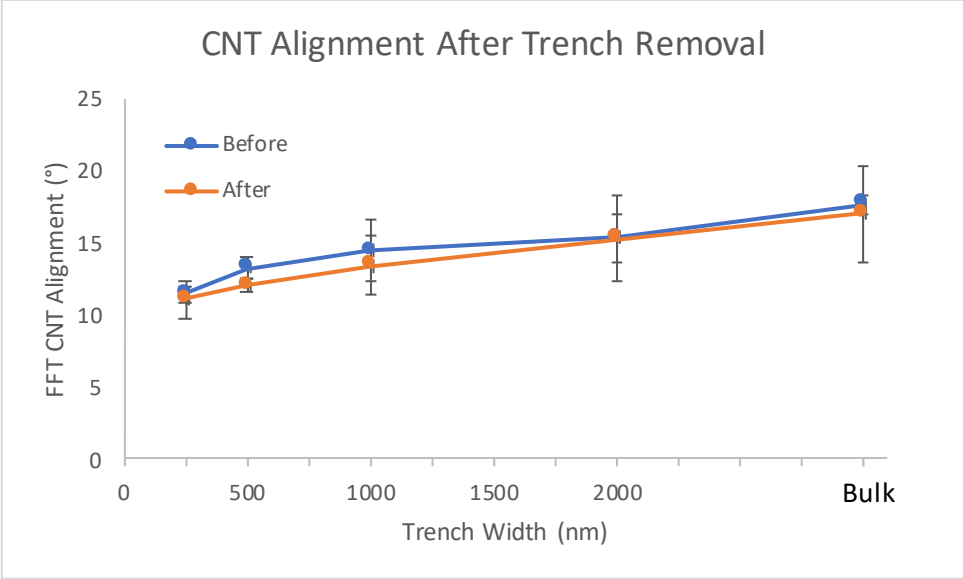

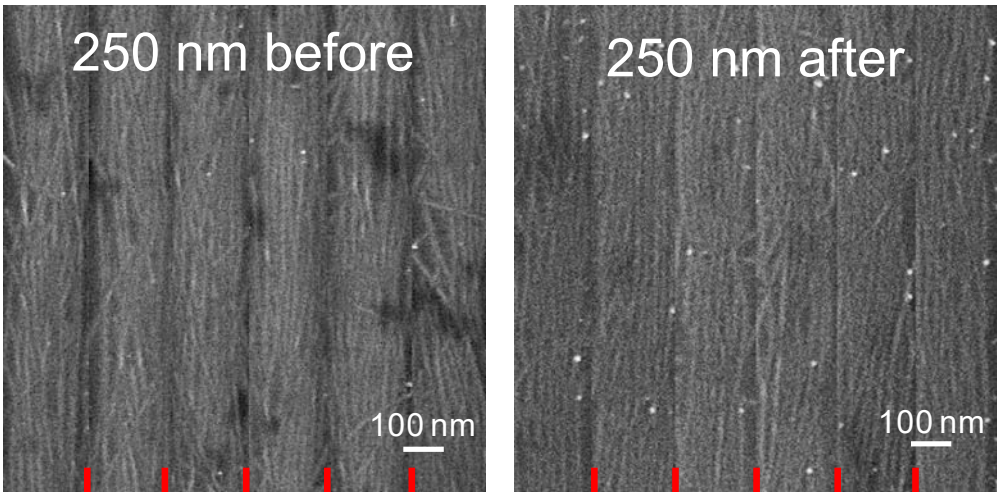

Figure S15. Plot showing the s-CNT alignment degree before and after trench removal. Below are stitched together s-CNT arrays from a SEM image of 250 nm wide trenches (left) before and (right) after removal.

CNT Removal from Gold Mesas

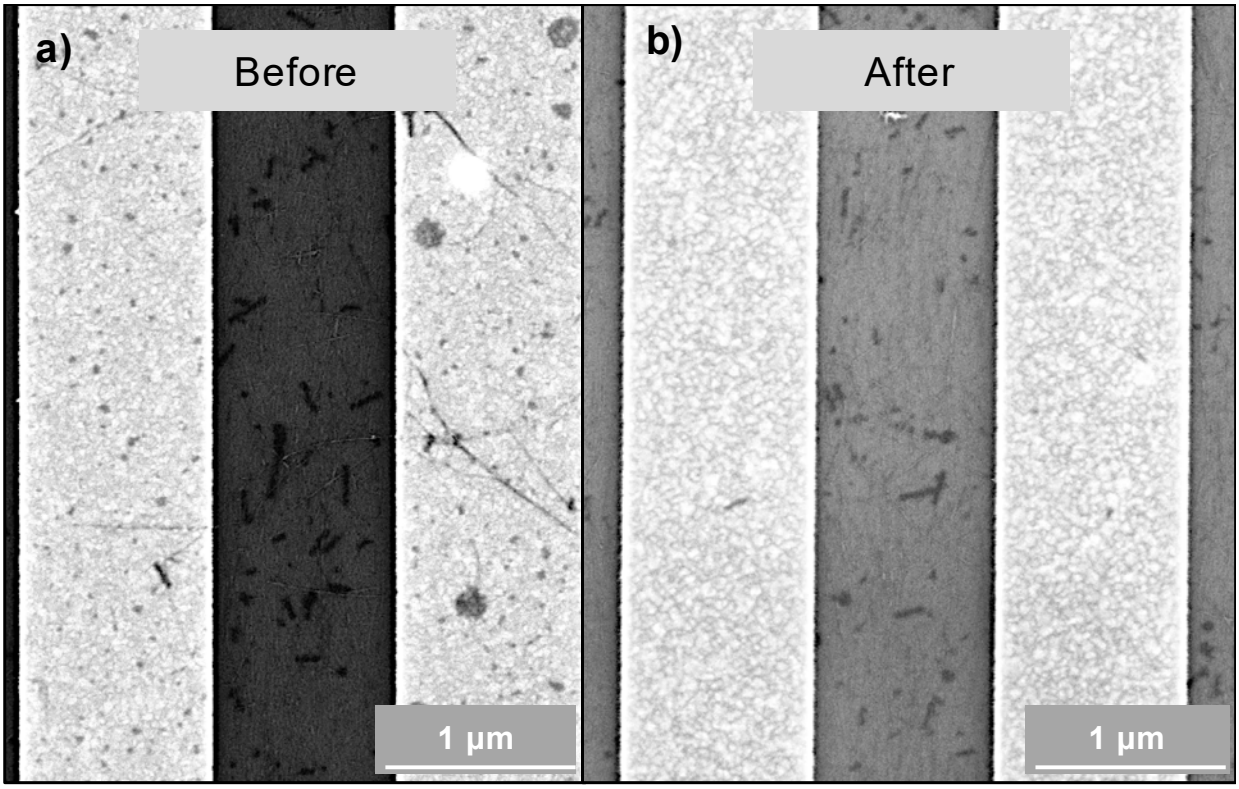

Figure S16. SEM images showing a 1-µm wide s-CNT array (a) before and (b) after the crossing CNTs deposited on OTh-grafted gold surface are removed via reactive-ion etching procedure. Scale bar of 1 µm is the same for both images.

CNT Electronic Properties after Trench Removal

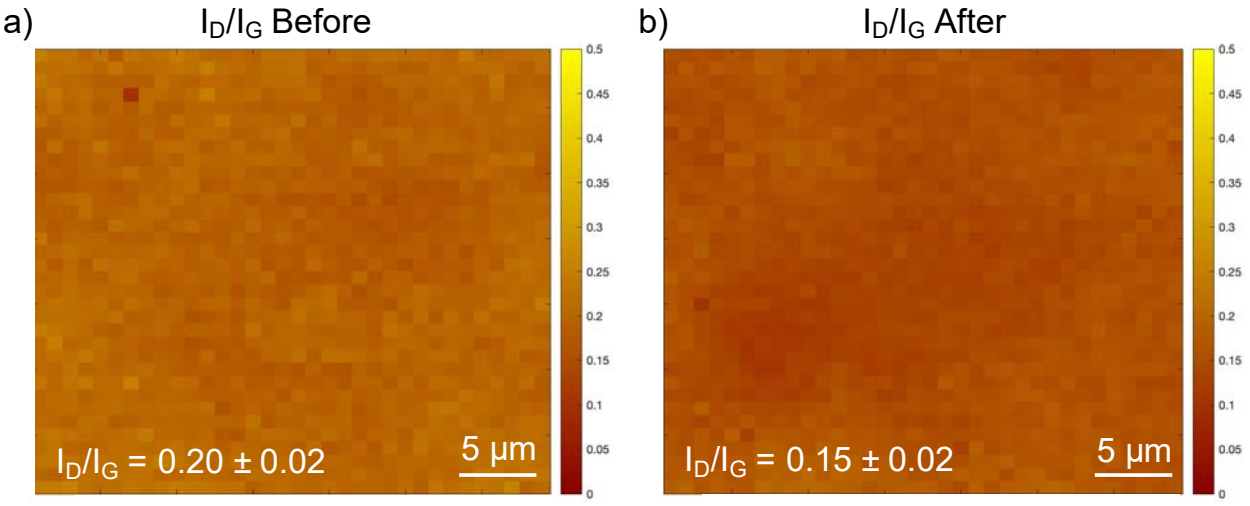

Figure S17. Raman maps of the ratio of the intensity of the D band to G band (I_D/I_G) for CNTs (a) before and (b) after the trench removal process over a 34 μm^2 area. The average value and standard deviation for each map is shown in the bottom left of each map. The averaged Raman spectra for each map showing the D, G, and 2D bands of the CNTs before and after the trench removal process, normalized to the Si peak, are shown in Fig. 4d of the main text.

Citations:

1. Kocabas, C.; Hur, S.-H.; Gaur, A.; Meitl, M. A.; Shim, M.; Rogers, J. A., Guided Growth of Large-Scale, Horizontally Aligned Arrays of Single-Walled Carbon Nanotubes and Their Use in Thin-Film Transistors. *Small.* **2005,** *1*, 1110-1116.
2. Joo, Y.; Brady, G. J.; Arnold, M. S.; Gopalan, P., Dose-Controlled, Floating Evaporative Self-assembly and Alignment of Semiconducting Carbon Nanotubes from Organic Solvents. *Langmuir.* **2014,** *30*, 3460-3466.
3. Liu, L.; Han, J.; Xu, L.; Zhou, J.; Zhao, C.; Ding, S.; Shi, H.; Xiao, M.; Ding, L.; Ma, Z.; Jin, C.; Zhang, Z.; Peng, L.-M., Aligned, high-density semiconducting carbon nanotube arrays for high-performance electronics. *Science.* **2020,** *368*, 850.
4. Dresselhaus, M. S.; Dresselhaus, G.; Saito, R.; Jorio, A., Raman spectroscopy of carbon nanotubes. *Physics Reports.* **2005,** *409*, 47-99.
5. Zhang, Y.; Zhang, J.; Son, H.; Kong, J.; Liu, Z., Substrate-Induced Raman Frequency Variation for Single-Walled Carbon Nanotubes. *Journal of the American Chemical Society.* **2005,** *127*, 17156-17157.

6. Carron, K. T.; Fluhr, W.; Meier, M.; Wokaun, A.; Lehmann, H. W., Resonances of two-dimensional particle gratings in surface-enhanced Raman scattering. *J. Opt. Soc. Am. B.* **1986,** *3*, 430-440.
7. Ayres, C. E.; Jha, B. S.; Meredith, H.; Bowman, J. R.; Bowlin, G. L.; Henderson, S. C.; Simpson, D. G., Measuring fiber alignment in electrospun scaffolds: a user's guide to the 2D fast Fourier transform approach. *Journal of Biomaterials Science, Polymer Edition.* **2008,** *19*, 603-621.
8. Morrill, E. E.; Tulepbergenov, A. N.; Stender, C. J.; Lamichhane, R.; Brown, R. J.; Lujan, T. J., A validated software application to measure fiber organization in soft tissue. *Biomechanics and Modeling in Mechanobiology.* **2016,** *15*, 1467-1478.
9. Brandley, E.; Greenhalgh, E. S.; Shaffer, M. S. P.; Li, Q., Mapping carbon nanotube orientation by fast Fourier transform of scanning electron micrographs. *Carbon.* **2018,** *137*, 78-87.